Available online at www.sciencedirect.com
ScienceDirect
Computers & Fluids 37 (2008) 218–235
computers & fluids
www.elsevier.com/locate/compfluid

Computational fluid dynamics (CFD) software tools for microfluidic applications – A case study

Thomas Glatzel [a], Christian Litterst [a], Claudio Cupelli [a], Timo Lindemann [a], Christian Moosmann [b], Remigius Niekrawietz [a], Wolfgang Streule [a], Roland Zengerle [a], Peter Koltay [a,*]

[a] *Laboratory for MEMS Applications, Department of Microsystems Engineering – IMTEK, University of Freiburg, Georges-Koehler-Allee 106, 79110 Freiburg, Germany*

[b] *Laboratory for Simulation, Department of Microsystems Engineering – IMTEK, University of Freiburg, Georges-Koehler-Allee 103, 79110 Freiburg, Germany*

Received 19 January 2007; accepted 2 July 2007
Available online 17 August 2007

Abstract

This paper reports on an exemplary study of the performance of commercial computational fluid dynamic (CFD) software programs when applied as engineering tool for microfluidic applications. Four commercial finite volume codes (CFD-ACE+, CFX, Flow-3D and Fluent) have been evaluated by performing CFD-simulations of typical microfluidic engineering problems being relevant for a large variety of lab-on-a-chip (LOAC) applications. Following problems are considered as examples: multi lamination by a split and recombine mixer, flow patterning on a rotating platform (sometimes termed ''lab-on-a-disk''), bubble dynamics in micro channels and the so called TopSpot® droplet generator for micro array printing. Hereby mainly the capability of the software programs to deal with free surface flows including surface tension and flow patterning of two fluids has been studied. In all investigated programs the free surfaces are treated by the volume-of-fluid (VOF) method and flow patterning is visualised with a scalar marker method. The study assesses the simulation results obtained by the different programs for the mentioned application cases in terms of consistency of results, computational speed and comparison with experimental data if available.

1. Introduction

Today CFD methods are well described in many textbooks [1,2] and applied routinely in engineering science. They serve as valuable tools for design and engineering of components and systems in turbo machinery, aerospace and many other fields [1]. In this paper we focus on the application of CFD as engineering tool for microfluidic devices and the particularities associated with it [3]. In micro dimensions, for example, surface forces dominate over body forces requiring special attention for problems involving two phase flows with free surfaces which are often driven by capillary forces. Typical flow situations are capillary wicking or formation of droplets which are characterised by low Weber and Reynolds numbers [4–6]. To model free surface flows including surface tension effects – amongst others – the so called volume-of-fluid method (VOF) has been established [7] and is still being refined [8–11]. Another particularity in microfluidics is the increased importance of diffusion for mixing phenomena. Since in microfluidic flow problems the Reynolds numbers are typically very small, turbulence is hardly ever observed and mixing is driven by diffusion only at low Peclet numbers [12]. Effective mixing within short times

* Corresponding author. Tel.: +49 761 203 7476; fax: +49 761 203 7539.
E-mail address: koltay@imtek.de (P. Koltay).
URLs: http://www.imtek.de/simulation/ (C. Moosmann), http://www.imtek.de/anwendungen/ (P. Koltay).

0045-7930/$ - see front matter © 2007 Elsevier Ltd. All rights reserved.
doi:10.1016/j.compfluid.2007.07.014

can thus only be achieved by decreasing the diffusion length of the fluids which can technically be realized by multi lamination or chaotic advection [13–18]. On the one hand the absence of turbulence in microfluidics simplifies the CFD treatment substantially but on the other hand diffusion is difficult to account for with the required accuracy in practical cases. High order discretisation schemes are required to suppress the so called ''numerical diffusion'' which is nothing else than numerical errors being accumulated by the algorithm.

Both of the described particularities, free surfaces as well as diffusion have been dealt with in length in the CFD-literature from a numerical point of view. In principle there are many approaches known to simulate these types of problems in more or less specific situations at various degrees of accuracy (see for example [11,13,19,20]). In this paper however, we want to assess the topic from an engineering perspective and ask the question: How helpful are the software tools being available for the micro engineer to address these problems in practice? As it is the nature of the selected engineering problems, they can not be solved analytically and thus have to be considered numerically with CFD. The crucial points in this context are the availability and the applicability of CFD-tools for engineering purposes in the considered cases. To do so a case study of various commercial CFD codes has been performed with respect to experimental results, where available. Due to the variety of commercial software tools and the limited resources for performing such case studies the authors restricted their choice to the four previously mentioned Finite Volume codes. A comparison to well established Finite Element codes like COVENTOR [21] or COMSOL [22] was not possible in the framework of this work.

Benchmarking in general is an essential part of CFD research and code validation [23–28]. However, due to the commercial nature of the software applied for the presented study, the algorithms are not in the public domain and are not know in detail. Therefore the presented case study can only be descriptive instead of analytic *i.e.* the outcome of the simulations can be documented and discussed but not be analysed in detail. Nevertheless, the state of the art of CFD simulation in microfluidics is presented by this approach and the question is addressed which tools are available and well suited for a specific purpose, if any. The devices studied in this paper were not selected for the purpose of driving certain numerical codes into problems, but are a representative selection of the problems encountered by the authors over the years in microfluidic research. Indeed, the major part of the paper deals with the application of simulation methods to these microfluidic devices that have not been published before. The results hopefully will provide guidance to micro engineers applying CFD as engineering tool as well as support for developers of CFD code in search of even faster and more accurate algorithms.

2. Approach

The approach followed in this paper is based on the assessment of selected simulation problems or cases which are considered to be typical and representative for microfluidic applications. Especially the diffusion at low Reynolds numbers and the aspects of surface tension dominated free surface flows have been considered for selection of the cases. Each of the four chosen problems presented in Section 4 in detail is simulated with each of the four selected CFD codes introduced in Section 3. The results of the simulations are compared to each other to assess the performance of the CFD-software as described briefly below and in more detail in Section 4. For the split and recombine mixer and the rotating channel it is important to point out that the focus was set on the flow patterns visualised by a tracer scalar value rather than real diffusive mixing. To suppress real physical diffusion and set the focus on the flow patterns the diffusion constant in the simulation program is set to a non-physical small value of $2E{-}20\ m^2\ s^{-1}$ which is considerably smaller than typical diffusion constants in real systems being in the order of $1E{-}10\ m^2\ s^{-1}$. As a side effect one obtains information about the strength of the numerical diffusion occurring in convective flows by transversal motion of the fluid with respect to the grid. To reduce the numerical diffusion in the simulations of bubble dynamics in micro channels and the TopSpot® droplet generator the VOF method with higher order discretisation schemes was applied [29].

The criteria for assessing the performance respectively the ''usefulness'' of a software tool for engineering purposes are naturally vague. Many objective factors as well as personal preferences play a role. Therefore the assessment of the performance is focused here on two main criteria which can be considered as impartial: First the consistency of results and second the computational speed. Consistency is mandatory to obtain predictive results applicable for engineering purposes and therefore the most important criterion. Furthermore, the higher the computational speed the more designs and variations can be tested within a given time frame, which enhances and facilitates the complete design process. In order to keep the results to be presented later on as comparable as possible with respect to these two main criteria, the authors have chosen to perform all simulations under conditions as identical as possible. This means especially that the same structured grid was used in all simulations and that transient simulations have been conducted with fixed and equal time steps. The authors are well aware of the fact that such conditions might not be ideal for those of the software codes showing their particular strengths in time step adaptation or by sophisticated grid generation techniques. On the other hand a predefined grid used by all codes provides the maximum control on the initial status of the numerical problem and focuses the attention on the core properties of the code like the discretisation scheme, the algorithm for pressure velocity coupling, methods for matrix solution etc.

Furthermore an appropriately predefined grid also assures that a grid convergent solution is attained and that the results are comparable and meaningful. In the presented cases it was confirmed using CFD-ACE+, that indeed a grid convergent solution could be obtained with the applied grid for all simulations.

3. Description of the applied hard- and software

In the present case study the software codes CFD-ACE+ [30], CFX [31], FLOW-3D [32] and FLUENT [33] have been investigated. All of the codes are based on the finite-volume method (FVM) [1] to solve the Navier–Stokes equations, except Flow-3D. Flow-3D is based on a combination of finite difference and finite volume perspectives and it uses a control volume approach to solve the conservation equations [23,24,34]. The velocity pressure coupling is generally accomplished by the SimpleC algorithm [1] which was original proposed by Vandoormaal and Raithby [35] or slight variations of it like the so called SOLA algorithm [34,36–39] applied by FLOW-3D. Furnished with these algorithms typical problems of incompressible laminar viscous flow can be addressed.

For the diffusion problems we have chosen to apply the particle tracking method supported by all of the programs. This method is sufficient to model diffusion within a liquid of uniform rheological properties and faster than two-fluid-methods. The particle tracking method is based on the advection of a scalar "marker" variable with the flow of a single homogenous fluid [2]. The scalar marker particles do not influence or interact with the flow. The scalar field serves to track how the initial distribution of marker particles is spread out and equilibrated by advection and diffusion only (*cf.* Eq. (1)), with ϕ being the tracked scalar value and S_ϕ a source term.

$$\frac{\partial \rho\phi}{\partial t} + \nabla \cdot (\rho \vec{u}\phi) = \nabla \cdot (D \nabla \phi) + S_\phi \tag{1}$$

For modelling free surface flows all of the codes apply the VOF method as proposed first by Hirt and Nichols [7] and refined later on by various authors [8–10,40,41]. It is based on tracking a scalar field variable F which stands for the distribution of the second fluid in the computational grid. F specifies the fraction of the volume of each computational cell in the grid occupied by the second fluid. All cells containing only fluid two will take the value $F = 1$, and cells completely filled with fluid one are represented by $F = 0$. Cells containing an interface between air and water take on a value of F between 0 and 1. For a given flow field with the velocity vector $\vec{v}$ and an initial distribution of F on a grid, the volume fraction distribution F (and hence the distribution of fluid two) is determined by the passive transport equation:

$$\frac{\partial F}{\partial t} + \nabla \vec{v} F = 0 \tag{2}$$

This equation must be solved together with the fundamental equations of conservation of mass and momentum, to achieve computational coupling between the velocity field solution and the liquid distribution. From the F distribution the interface between the two fluid phases has to be reconstructed at every time step. All programs except CFX are using the piecewise linear interface construction (PLIC) scheme [9] for this purpose. CFX does not apply any surface reconstruction because it computes free-surface flows on unstructured meshes, where surface reconstruction is computationally expensive. To overcome numerical diffusion and a smearing of the interface a "compressive scheme" is applied instead [42].

The position, shape and especially the curvature of the free surface are required to determine the capillary forces given by the Young-Laplace equation [1,2,43–45]. Typically these surface forces are included into the algorithm as body forces in those cells containing the interface *i.e.* having F-values between 1 and 0 [7,9]. Contact angles at the fluid/solid interface are accounted for in a similar way [11].

For solving the algebraic equations typically two types of solvers are applied in the commercial codes: The adaptive multi grid solver (AMG) and the conjugate gradient solver (CGS) [46,47].

3.1. CFD-ACE+

Version 2004.0.25 of CFD-ACE+ (ESI-CFD, Inc., Huntsville, AL) was applied for this study, which is claimed to be an integrated software package for multiphysic computational analysis [30]. The program consists of three main parts, CFD-GEOM for geometry and grid generation, CFD-GUI for setting boundary and initial conditions and CFD-VIEW as an interactive visualization program. All tools can be controlled by the Python [48] scripting language to enable automatic batch operations.

CFD-GEOM is the built in geometry and grid generation system with a large set of CAD-functions to create and manipulate whole geometries with a subsequent meshing. After setting up the geometry the appropriate solver settings can be chosen in CFD-GUI where the solvers for different physical problems are divided into so called modules specifying the kind of physical problem which can be switched on and off separately. Most of the modules can be combined with others giving the opportunity to simulate different physical domains at the same time, *e.g.* flow problems in combination with chemical reactions, free surfaces etc.

The VOF method in CFD-ACE+ offers some additional features like an algorithm to remove the so called flotsam and jetsam. This is an effect caused by numerical errors, and is characterised by the generation of tiny isolated droplets of liquids or gas in the regions of the other medium, especially in regions of high swirl. A further feature is given by the capillary-wave damping which allows for locally increasing the viscosity in the vicinity of the interface

enabling larger time steps since tangential velocities are reduced. As mentioned in the manual of CFD-ACE+ [30] for the surface reconstruction three methods are available, a 0th order scheme, an upwind scheme with the SLIC method and an upwind scheme with the PLIC method [49].

3.2. CFX

For the presented case study version 5.7.1 of the CFX CFD-software was used [31]. For the task of grid generation there are two tools available: ANSYS DesignSpace in combination with AI*Environment [50] and ICEM CFD [51]. In contrast to other tools, both ANSYS Workbench and ICEM CFD cannot be controlled via a scripting language; ANSYS Workbench however can handle parameterized geometries. ICEM CFD has only basic modelling capabilities, but supports a wide range of mesh operations and mesh types.

To define physical properties such as material properties and boundary conditions as well as solver settings the preprocessor CFX-Pre is provided with the CFX package. Both CFX-Pre as well as the postprocessor, CFX-Post can be either controlled with the CFX-Expression-Language (CEL) or with Perl scripting. The CFX-solver can handle multiphase flows of any number of different fluids, where fluids can be gases or liquids and all material properties can either be constant or dependent on any variable in the simulation. All problems can be calculated on structured and unstructured meshes.

Like most CFD-tools CFX also uses the finite-volume method for spatial discretisation, however, the VOF method for free surfaces is implemented in a different way. No surface reconstruction is applied but the volume fraction is computed based on solving an artificially stabilized (''compressive scheme'') advection equation [42]. Surface tension can also be accounted for, and it is computed based on the local gradient of the VOF variable. In contrast to the other tools CFX does not use a segregated solver for flow speed and pressure, but a fully coupled solver. CFX can perform all types of simulations on multiple processors, where parallelisation can be achieved using MPI (message-parsing interface [52]) or PVM (parallel virtual machine) [53].

3.3. Flow-3D

Flow-3D from Flow Science, Inc. [32], Solver Version 8.2.5 and Interface Version 4.0.0 were used for this case study. The Flow-3D package consists of a graphical user interface (GUI) and a separate tool called Flow-VU for meshing and handling external STL files of three-dimensional geometries. The pre- and post-processing as well as the study of the simulation results is done by Flow-VU. The multi processor capable solver can handle different physical regimes and for example compressible and incompressible flow situations, and one- or two-fluid problems with a free surface.

The meshing procedure in Flow-3D is based on a multiple block meshing, either hexahedral grids in a cartesian coordinate system or cylindrical grids in a polar coordinate system. In multiple block meshing the geometry is superimposed by independent meshed-domains or blocks with domain interfaces connected by a specific interpolation function. This is different from all other simulation tools discussed here, where the meshing method is more like building up a geometry with structured or unstructured nodes, lines, surfaces and blocks. The main advantage of the multiple block meshing is the possibility to refine a mesh dependent on the required spatial accuracy and independently of the geometry, a feature especially interesting in microfluidic applications with large aspect ratios. A disadvantage is that only structured grids can be handled and furthermore these multiple block meshes are not compatible for exchange with most other solvers.

The applied numerical solution algorithms are based either on the finite-difference [1] or the finite-volume method [2,34]. Free surface problems can be solved using the implemented VOF method including surface tension and applying standard VOF solution methods as well as a new Semi-Lagrangian VOF advection method [7,37,39]. The proprietary approach of Flow-3D called Semi-Lagrangian advection method [37], which is used throughout the presented simulations, consists of three basic steps. First, the approximation of the fluid interface in a cell with a planar surface, second the movement of the fluid volume according to the local velocity field, and third the computation of the new fluid fraction values in the computational cells using an overlay procedure. For this algorithm Flow-3D only supports automatic time-steps and no fixed time steps. This makes it difficult to compare Flow-3D with the other tools concerning computation time. A further remarkable fact is that all problems have to be calculated time dependent because Flow-3D does not provide the possibility of steady state simulations.

3.4. Fluent

Fluent version 6.1.22 from Fluent Inc. [33] was used for this case study. The whole Fluent software package includes the Fluent solver with only few limitations concerning mesh-types, the pre-processor Gambit (version 2.1.2) for geometry modelling and mesh generation as well as an additional pre-processor called TGrid for generating volume meshes from existing boundary meshes.

For the geometry creation Gambit provides a common set of CAD-functions as well as a built-in scripting functionality that allows for a fast geometry creation. Gambit provides structured (quadrilateral in 2D and hexahedron, prism/wedge in 3D), unstructured (triangle in 2D and tetrahedron, pyramid in 3D), hybrid and non-conformal meshes. Structured meshes can either be created manually or by using the Cooper-scheme [54] allowing for a fast meshing with good grid quality.

After an appropriate mesh is provided, Fluent is used for the simulation setup, the solving process and the post-processing of the results. During the simulation setup all GUI-commands are scripted by the program but one has to be aware of the fact that not all possible settings are accessible by the GUI. Some special functions are only available if entered on the command line level leading sometimes to difficulties in finding the appropriate settings.

In general, Fluent is able to solve all the problems discussed in this paper on structured and unstructured meshes. Regarding the VOF model Fluent provides four different VOF-formulations: the geo-reconstruct scheme (comparable to PLIC), the donor-acceptor scheme (comparable to SLIC), the Euler explicit and the implicit scheme [55].

3.5. Hardware

All simulations were performed on a dual-Athlon MP-1900 PC running MS Windows 2000 Professional, SP4 delivering 3.8 Gflops. At no time the memory occupation of the simulations exhausted the available memory of 1 GB. The simulation times displayed in this publication were determined by a small program running on this machine logging the accumulated user and system time by the use of Sysinternals PsList [56]. Also the memory utilisation was recorded for both user and system space and is displayed later on in this publication.

4. Simulations and results

All simulation problems discussed in the following were simulated on a structured grid as motivated in the beginning. Transient simulations were performed in an explicit formulation using a first order Euler scheme with fixed time steps, except for Flow-3D were an automatic time step had to be used as described in the previous section. The VOF method is treated by all tools in an explicit way except for CFX which uses a so called high-resolution scheme with an implicit second order Euler scheme.

Generally water and air have been chosen as fluids with their physical properties taken from the CFD-ACE+ material database [57] since water and water solutions are still relevant for many real systems (e.g. for the considered TopSpot device). Considering a larger selection of different liquids or liquids with special rheological properties would require a lot of additional computational time. Therefore the study has been focused on four different devices instead of an extensive analysis of fluid parameters. All fluids were treated as being incompressible which is justified for the small pressure differences occurring in the examples. If not indicated otherwise first or second order upwind schemes were applied for discretisation. In problems involving free surfaces the VOF method with PLIC surface reconstruction and surface tension was applied except for simulations with CFX.

Finally AMG respectively CGS methods were used for solving the numerical equations. Further details of the four selected problems like computational grid, boundary conditions (BC), initial conditions (IC) etc. are given in the following subsections.

4.1. Split and recombine mixer (flow patterning)

Mixing is an essential step in many Lab-on-a-Chip devices. Due to the laminar nature of the flow in micro dimension mixing is mainly achieved by diffusion instead of advection. A common method to enhance mixing is to reduce the diffusion length via so called multi-lamination principles. In Fig. 1a and b a split and recombine mixer [16] is shown that doubles the number of fluid lamellae in each split-and-recombine step and thus enables more efficient mixing. Numerical simulation of mixing even under laminar conditions usually results in high cell Peclet numbers: $Pe = \rho u \delta x / D$, where ρ is the density of the fluid, u

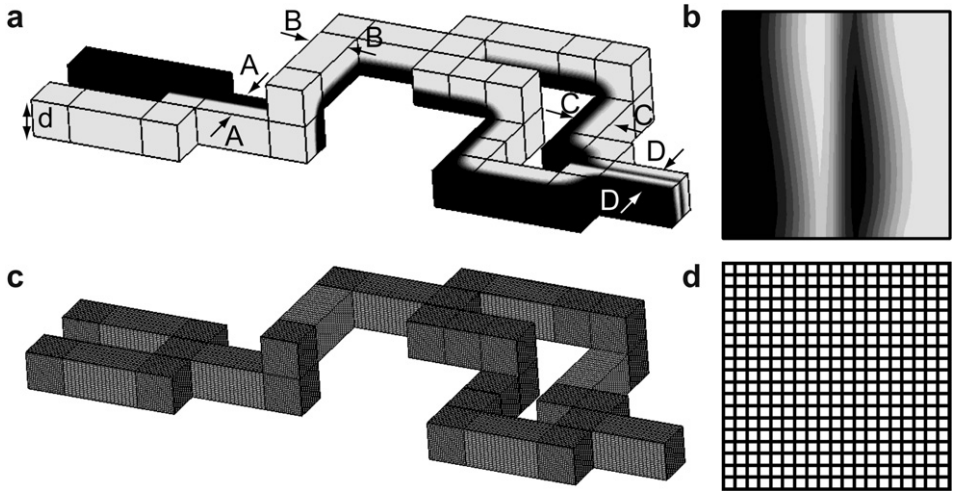

Fig. 1. Model of the split and recombine mixer: (a) full model displaying the simulation result; (b) cross section at position C–C exhibiting four fluid lamellae; (c) full view of the structured grid; (d) cross sectional view of the grid at position A–A.

is the velocity, D is the diffusion coefficient of the generalised transport equation and δx is the dimension of the numerical cell. For high cell Peclet numbers the numerical diffusion constant, *i.e.* diffusion due to numerical errors, is comparable or even larger than the real diffusion to be studied in the simulation. In order to achieve a sufficient numerical accuracy the numerical diffusion has to be reduced by using an adequate grid resolution and high order differencing schemes [1,2].

4.1.1. Problem set-up

The first setup for the investigation of mixing under laminar conditions as sketched in Fig. 1a is composed of square channels with a side length of $d = 500$ μm. The structured grid of the mixer consists of 226,347 cells with quadratic base area with a side-length of 26.3 μm and a maximum cell aspect ratio of 1:2 (*cf.* Fig. 1c and d). The boundary conditions for the steady state simulation were set to a constant velocity of $v = 0.001\ \mathrm{m\ s^{-1}}$ at the two inlets and to a constant pressure of $p = 0$ Pa at the outlet. This yields $Re \approx 1$ and is thus located in the transition region between creeping and laminar flow. Initially the whole model was filled with water, whereas water entering through the left inlet was marked with tracer particles (coloured in black $\phi = 1$ in Fig. 1a) to visualize the flow pattern. By setting the diffusion constant of the tracer to a value of $2\mathrm{E}{-}20\ \mathrm{m^2\ s^{-1}}$ the blur of the interface in all simulations is caused by numerical diffusion only. Real physical diffusion can be neglected on the considered time scale for this small diffusion coefficient. While in real parallel lamination micro-mixers the Peclet number is in the order of 10 to 2E+5 [12] in the presented simulation the number is in the order of $Pe = 5\mathrm{E}{+}13$. In the real systems the mixing is dominated by diffusion, indicated by the small Peclet numbers while in the simulation the Peclet number is high and thus the physical diffusion is suppressed.

In case of Flow-3D a two step procedure has been used. First a transient simulation was performed until the velocity profile reached a steady state, i.e. no change of local velocity vectors between two subsequent time steps. In a second step this solution was used for the steady state propagation of the scalar ϕ, i.e. solution of Eq. (1).

4.1.2. Total pressure drop

The correctness of the pressure drop across a fluidic structure at a given flow rate, *i.e.* the fluidic resistance, is one of the central requirements for consistent simulation results. According to Hagen-Poiseuille's law a linear pressure drop is expected over a simple straight channel. For a complex geometry like in this problem however, the pressure drop is hardly predictable because a fully developed Poisseuille flow is not established and additional pressure losses in constrictions and turns have to be considered. A rough analytical estimation by summing up the pressure drops across the straight channel segments assuming Poisseuille flow underestimates additional pressure drops in corners and results in a pressure of ~1.3 Pa compared to the simulation results shown in Table 1 of approximately ~1.8 Pa. Since the flow in the considered geometry is dominated by entrance effects occurring at the bends and the changes of the cross-section the problem can not be fully solved adequately in an analytical way. These effects add to the resistance in a complex way which requires a full CFD treatment to obtain a quantitative solution and also explains the difference between the very simple model and the CFD-results. The pressure drops calculated with three of the CFD tools are in good agreement and deviates less than 1% from each other. The only exception is Flow-3D where the deviation is ~5% compared to the results of the other programs (*cf.* Table 1). Though no experimental data is available for validation in this case, it can still be assumed due to greatly consistent simulation results that a pressure drop of about 1.8 Pa at a mean flow velocity of $0.001\ \mathrm{m\ s^{-1}}$ comes close to the real value.

Table 1
Pressure drop over the split-and-recombine structure

Tool	Resulting pressure drop in (Pa)
CFD-ACE+	1.801
CFX	1.795
Flow-3D	1.710
Fluent	1.799

4.1.3. Qualitative lamination pattern

The qualitative lamination patterns of the mixer were analysed using a scalar marker with a numerical diffusion coefficient of $2\mathrm{E}{-}20\ \mathrm{m^2\ s^{-1}}$ which is too small to create real physical diffusion as mentioned before. Two aspects of the simulation results can be tested by this method. First, the smearing of theoretically nearly infinitely sharp interface provides information about the extent of numerical diffusion. A high numerical diffusion results in a more pronounced blur of the interface, whereas a high degree of numerical accuracy leaves the interface undistorted. Second, the scalar field provides also a check of the correctness of the calculated flow field, since the streamlines of the flow determines the lamination pattern. Thus, for the considered problem, identical lamination patterns provided by different simulation tools prove the consistency of the underlying flow fields.

In Fig. 2 the results of the lamination pattern are displayed for different positions along the mixer as indicated in Fig. 1. The results show that all codes calculate the flow field correctly and consistently with a comparable amount of numerical diffusion. Only slight qualitative differences can be detected: The initial lamination (A–A) is (practically) identical for all codes. After the first twist (cross-section (B–B)) slight differences are visible. ACE+ and CFX show no significant deviation, while Flow-3D shows a residual amount of white liquid ($\phi = 0$) in the corners as a result of the used methodology. Fluent shows a slightly different interface region. The cross-sections (C–C) and (D–D) show a corresponding behaviour. Overall all tools provide satisfactory and very similar result.

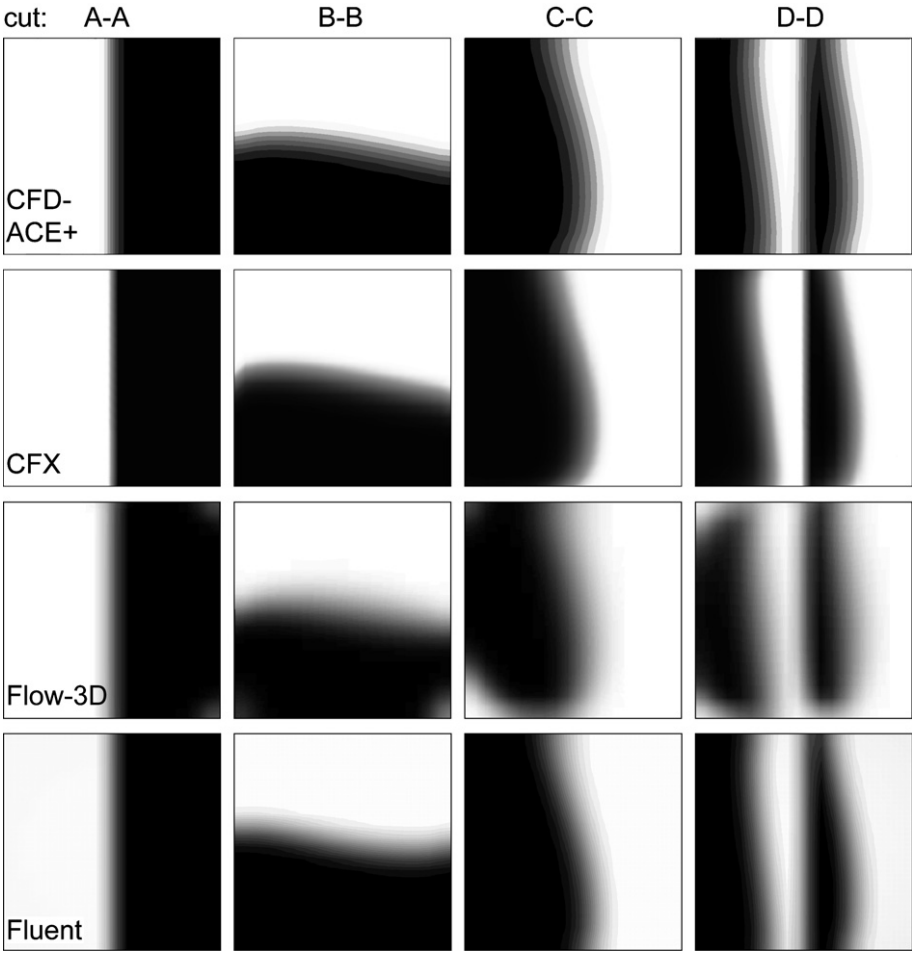

Fig. 2. Lamination pattern after successive segments of the mixer unit from left to right (*cf.* Fig. 1): first combine step: (cut A–A), after first twist (cut B–B), after second twist (cut C–C) and at the outlet (cut D–D).

4.1.4. Comments on the simulations (split and recombine)

It was possible to model the problem of the split recombine mixer with all simulation tools. However, for Flow-3D a stationary simulation could not be conducted for the problem. Instead the simulation was performed as follows: First for a simulation time of 1.1 s a transient run was calculated for establishing a stationary velocity profile. Afterwards the calculated flow field was used to transport the scalar marker in a transient run of 3.4 s assuming a constant velocity profile. This means that the stationary problem was simulated by a transient run of 4.4 s in total.

For all simulation tools a higher order upwind scheme for the solution of the diffusion/convection Eq. (1) was available and applied. Due to this the numerical diffusion was reduced by all codes to an acceptable amount.

4.2. Mixing in a rotating channel (flow patterning in rotating system)

Rotating CD-like formats are very prominent in microfluidics, especially for realizing LOAC devices [58,59]. Making use of the centrifugal force liquid can be pumped through microfluidic structures on rotating disks. Similar to a pressure driven flow, the centrifugal force induces a parabolic flow profile pointing in radial direction. Due to the velocity-dependent Coriolis force additionally an inhomogeneous transversal force field is generated in tangential direction which has its largest value in the centre of the channel. This leads to a transversal motion of the fluid in radial channels finally leading to a convective flow [60]. In the present problem the lamination induced by this convection is studied which is of special practical importance for the CD-based high throughput mixer proposed by Haeberle et al. [61] and Ducreé et al. [62].

4.2.1. Problem set-up

The simulations are performed in the rotating reference frame where the channel walls remain at rest, *i.e.* the reference frame rotates at the speed of the disk. For this kind of simulation it is crucial for all simulation tools that the boundary conditions are properly transferred into the rotating frame.

The 3D simulations were carried out for a channel of $l = 10$ mm in length pointing in radial direction and starting at a distance of $R = 20$ mm from the centre of rotation as sketched in Fig. 3a. The cross section is $a = b = 200$ μm

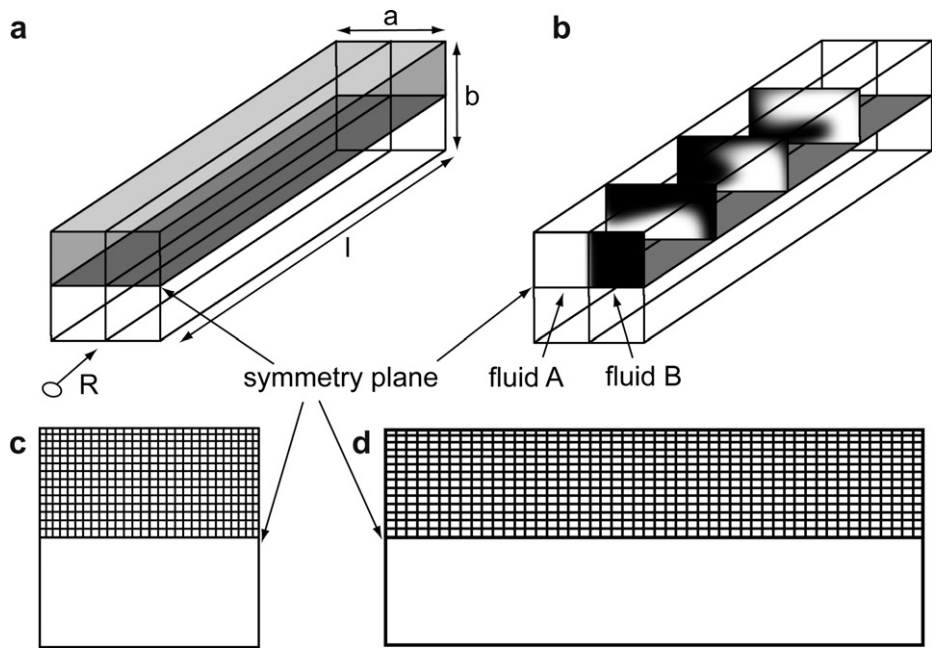

Fig. 3. (a) Radial square channel with symmetry plane. (b) Convection patterns of fluid A and B along the channel. Pictures are taken every 2.5 mm. (c) Mesh of the cross section of the channel with 29 nodes in each direction and a power law of 1.1. (d) Mesh of the first 500 μm in the direction of the channel.

with the symmetry plane in the middle of the channel. To save computation time the simulation was performed on the structured grid displayed in Fig. 3c and d which exploits the planar symmetry of the problem. The total channel has 1000 uniformly distributed nodes along its length, 15 respectively 29 nodes along its height and width resulting in 391,608 cells. The stationary simulation was performed with non-slip boundary conditions at the walls and a constant pressure boundary condition of 0 Pa at the inlet respectively outlet. Initially the whole channel was filled with water whereas the right half of the inlet was set to provide the scalar marker (Fluid B) to determine the convection patterns as in the previous example.

4.2.2. Flow rates and pressure drop along the channel

An appropriate quantitative measure to assess the simulation results for this problem is the variation of the pressure in the centre of the channel as a function of radial position. Unlike for pressure driven flow the pressure drop along the rotating channel is not linear. Due to the increasing centrifugal force the pressure increases further away from the centre of rotation. This results in the well known convex pressure profile as displayed in Fig. 4 [63].

Though there are neither analytical solutions nor experimental data available for validation in this case, it seems like that the most plausible result is produced by CFX. The pressure curve starts with $p = 0$ Pa at the inlet, decreases in a convex way and finishes at $p = 0$ Pa at the outlet, which is consistent with the basic physical interpretation of this model. Amazingly Fluent and Flow-3D fail to maintain $p = 0$ Pa at the inlet which should be given by the boundary condition at this point. In addition to this offset, Fluent provides a solution with an unexpected overshoot

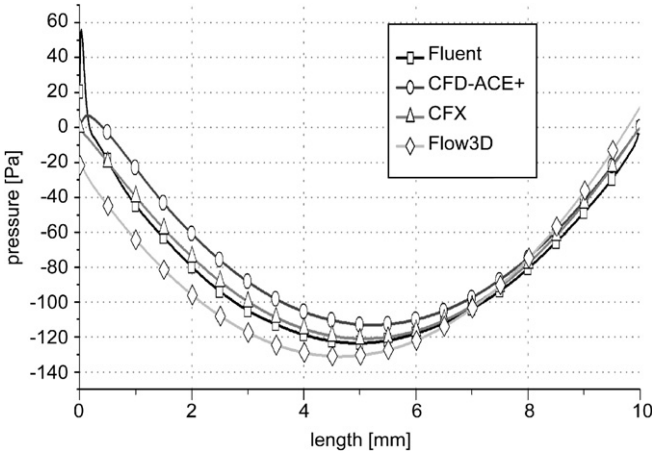

Fig. 4. Pressure distribution along the channel centre from inlet (0 mm) to outlet (10 mm).

within the first 200 μm length which cannot be explained even qualitatively by the underlying physics. Such an overshoot is also present in the results produced by CFD-ACE+, though it is considerably smaller and the solution is at least consistent with the boundary conditions at the inlet and outlet. Apart from the deviations at inlet and outlet, all of the results are more or less consistent within ±20 Pa. The consistency even improves at the distant end of the channel, which suggests that the deviations between the codes might diminish for larger distance from the centre of rotation. However, this remains to be confirmed by a more detailed study.

The resulting overall flow rate was determined to be about 16 μl s^{-1} leading to a Reynolds number of $Re = 95$ by all of the codes except Flow-3D where only a flow rate

of 3 μl s^{-1} was calculated. This is especially surprising because the convective flow patterns (*cf.* Fig. 5) are in good agreement with the other tools, and this should indicate a similar flow rate because the convective stirring of the fluid is highly dependent on the flow rate inside the channel.

4.2.3. Qualitative lamination pattern

The qualitative assessment of the lamination pattern displayed in Fig. 5 reveals that in all codes the Coriolis force is considered correctly in principle. Convection occurs perpendicular to the channel axis leading to a folding of the two fluids. The convective mixing patterns are quite similar for all simulation tools, but do not correspond to each other exactly. Due to the lack of experimental data it cannot be determined which of the results is closest to reality. Nevertheless, the overall quality can be assessed in terms of the numerical diffusion as before. As far as this can be judged due to the different visualisations, also in this case the extent of numerical diffusion can be considered similar for all tools and to be appropriate for the applied second order scheme.

4.2.4. Comments on the rotating channel simulations

The fluid dynamics occurring in a rotating channel seems to be qualitatively well reflected by all of the software tools (Table 2). All of the flow patterns are quite consistent. Therefore it is very likely that also experimental results will correspond to the given flow pattern qualitatively. Thus it should be possible to predict mixing qualitatively by any of the software tools as long as the diffusion constants are high. To which extent such mixing can be described quantitatively has to be determined in a more detailed study.

Table 2
Flow rates in the rotating channel

Tool	Flow rate (μl min^{-1})
CFD-ACE+	16.30
CFX	15.65
Flow-3D	3.00
Fluent	15.16

The pressure drop along the channel could not been calculated to full satisfaction. Apart from quantitative deviations between the various tools also qualitatively unphysical pressure curves have been obtained. Only CFX did not exhibit either non-convex solutions or a considerable offset. This is somewhat amazing since the pressure drop was determined assuming overall laminar viscous flow which typically can be calculated very precisely by CFD.

For the presented case Flow-3D and Fluent did not provide a direct steady state solution but instead the steady state had to be found by iterative simulations. In case of Flow-3D it was necessary to perform a transient simulation until the velocity profile was established. After that a further simulation did follow assuming a constant velocity profile to push the user scalar through the whole channel providing the entire lamination pattern. For Fluent the solving process was a sequence of steady state simulations where the pressure at the inlet had to be adapted manually step-by-step because Fluent was not able to solve the prob-

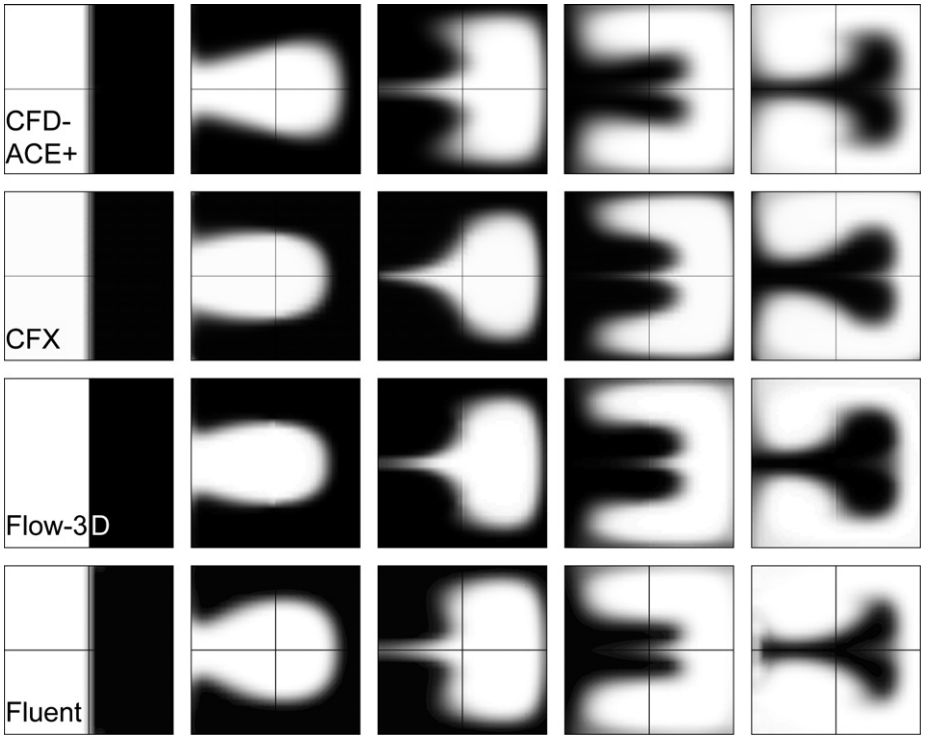

Fig. 5. Perpendicular cut along the channel at different positions. The marker particles visualize the convection and folding which occurs perpendicular to the channel direction.

lem correctly with an inlet pressure boundary condition of 0 Pa and zero flow. The first initial simulation was done with the 0 Pa pressure boundary condition leading to a negative pressure at the inlet. Using these flow patterns in a second simulation and correcting the negative total pressure value by adding this offset value to the inlet gauge total pressure boundary condition. After four of these iterations by subsequently adding the pressure values the resulting pressure at the inlets was below 10 Pa and after eight iterations below 1 Pa. This iterative simulation process is definitively a drawback of this tool which only occurred in solving this special case in a rotating reference frame. It should be noted that this simulation procedure was proposed by the support of Fluent.

4.3. Bubble dynamics in T-shaped channels (equilibrium VOF problem)

The T-shaped channel geometry as depicted in Fig. 6a can be applied to enhance the mobility of gas bubbles trapped in micro channels [64,65] and to inhibit clogging of the microfluidic channels. The mobility can be maximised by choosing appropriate geometrical dimensions for the channel as well as taking the contact angle Θ between the wall and the fluid into account. For contact angles of $\Theta < 90°$ a gas bubble can adopt three stable positions in such a T-shaped channel, depending only on the channel dimensions. These positions are referred to as horizontal, blocking and vertical motivated by the shape of the bubble if observed through the channel cross-section. This type of structure has been applied for example in an electronic fountain pen [66] and with a modified channel geometry for micro direct methanol fuel cells [67].

4.3.1. Problem set-up

The aim of this problem is to determine the equilibrium shape and position of an air bubble in the water filled channel for three channel designs (*cf.* Table 3) at a defined contact angle of $\Theta = 5°$. Since the only driving force in the system is the capillary force of the free surface the solver has to deal with very small driving pressures. Therefore a good implementation of the surface reconstruction and contact angle treatment is of importance to achieve the correct stable bubble shape.

Since the geometry of the channel as well as the simulation problem itself is fully symmetric, the model can be reduced to the geometry shown in Fig. 6b. This reduces the number of cells and allows for faster computation. The whole problem is considered to be in a closed volume with no fluid inlet or outlet. Thus the only boundary conditions applied are the symmetry and wall boundaries shown in Fig. 6c. The number of cells in the computational grid changes for each design as given in Table 3. As an initial condition an air bubble of spherical shape was placed in the centre of the model having a gas volume of 380 nl in all of the designs [65].

4.3.2. Qualitative shape of the bubble

The main criterion to assess the results of simulation problems involving free surfaces is the qualitative shape of the free interface. In the considered case the interface is formed by a gas bubble enclosed in a micro channel. Due to the T-shape of the channel the bubble can take on different configurations, depending on the geometrical dimensions. Depending on the equivalent hydraulic diameter of the channel either a horizontal, vertical or fully blocking position of the bubble is attained driven by the

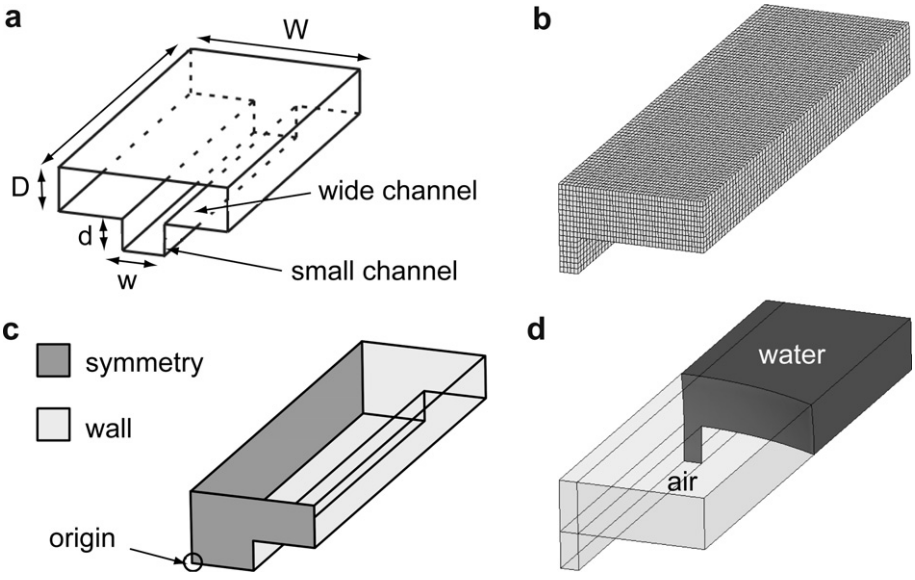

Fig. 6. (a) T-shaped channel with corresponding geometrical parameters. (b) Computational grid used for the simulations (design 1). (c) Applied boundary conditions (contact angle $\Theta = 5°$). (d) Initial conditions defined by the spherical gas bubble centred in the lower left corner of the mesh indicated by (origin) in (c).

Table 3
Geometrical and grid data for the three designs. The numbers in brackets signify the grid dimensions *i.e.* the length of a single grid cell

	Parameter					Number of cells
	w (μm)	W (μm)	d (μm)	D (μm)	l (μm)	
Design 1	125(0.096)	1000(0.098)	125(0.064)	175(0.063)	3500(0.04)	34,845
Design 2	250(0.104)	1000(0.098)	125(0.064)	175(0.063)	3500(0.04)	38,916
Design 3	500(0.108)	1000(0.014)	125(0.064)	175(0.063)	3500(0.04)	47,058

minimisation of the surface energy. The equilibrium positions for the three studied designs displayed in Fig. 7 were obtained from the initial condition after capillary oscillations have been completely damped. This was achieved approximately after 8 ms of simulation time for most of the software tools, except for Flow-3D where 20 ms of simulation time were necessary to obtain a sufficiently stationary result.

The qualitative comparison of the simulated bubble shapes with the experimental results displayed in Fig. 7 reveals that the consistency is best for CFD-ACE+ and Fluent which predict all shapes essentially correctly. CFX as well as Flow-3D manage to predict the qualitative bubble type correctly (vertical, horizontal or blocking) but are less accurate with respect to the curvature of the menisci. Especially the top view of the channels exhibits noticeable deviations between experiment and simulation. This can be explained for CFX by the different surface reconstruction method as explained in the previous sections. For Flow-3D the reason for the deviation remains unclear.

4.3.3. Comments on the simulations (T-shaped channel)

Flow-3D did not allow for setting the time steps constant. Thus the computational time is not directly comparable to the other programs.

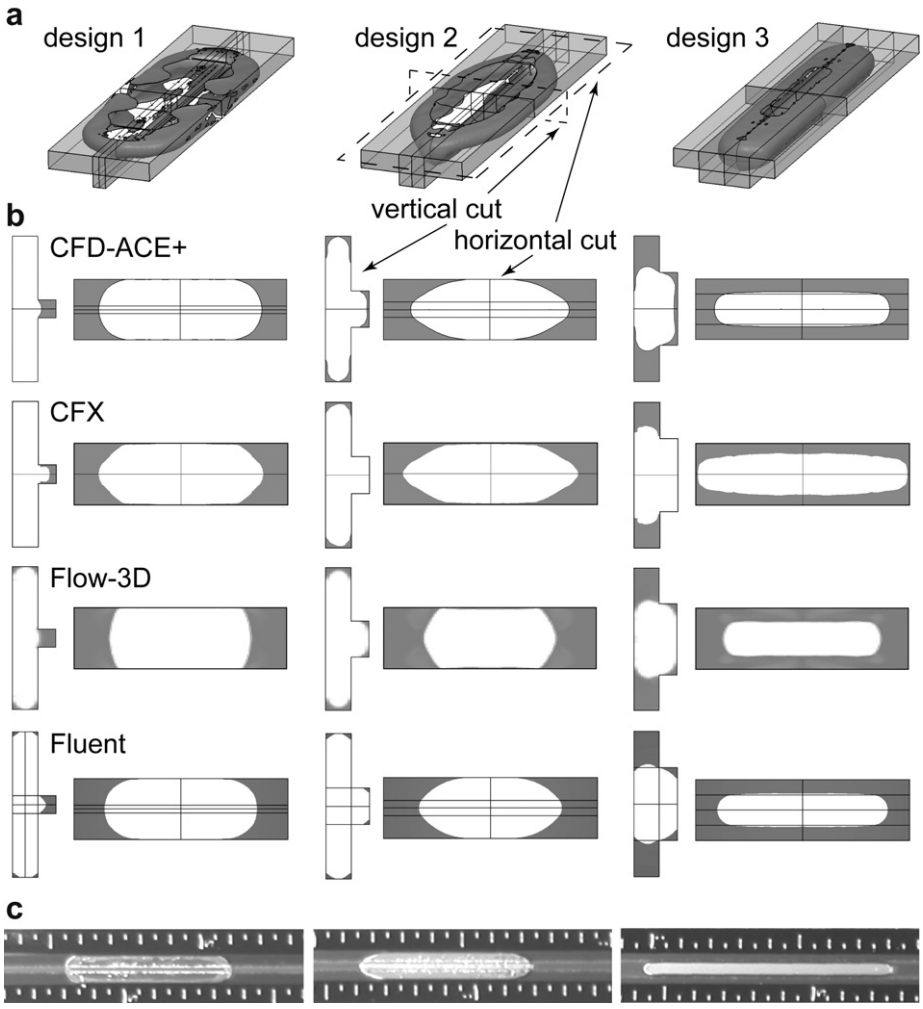

Fig. 7. (a) Three dimensional (3D) view of the T-shaped channel, (b) simulation results for designs 1 to 3 (water is depicted grey, air is displayed white) and (c) photographs of experiments.

4.4. TopSpot® micro arrayer (dynamic VOF problem)

Micro droplet generation has always been an essential benchmark for testing CFD codes [26–28,42,68]. In this paper we consider the TopSpot® [69] micro arrayer technology for this purpose. Micro arrays are highly parallel biosensors enabling a fast and parallel detection of thousands of different biochemical substances in one single experiment making it a key technology in many fields of basic research, diagnostics and drug discovery [70,71]. The sensor effect is based on an observable chemical reaction between arbitrary test specimens and immobilized molecules printed in a regular array on a glass slide. With the TopSpot® Technology whole micro arrays can be fabricated in one single step by printing hundreds of substances at the same time while the droplet ejection is actuated by an external pressure pulse.

4.4.1. Problem set-up

A fully three-dimensional simulation model of one single micro nozzle of a TopSpot® printhead (*cf.* Fig. 8) was set up to study the droplet generation applying the VOF method. In contrast to the static equilibrium problem of the T-shaped channel (*cf.* previous section), the droplet ejection by the TopSpot® method is a fully transient problem requiring considerable simulation time.

The grid model of the TopSpot® (*cf.* Fig. 8a) contains a single micro nozzle with a diameter of 50 μm and a length of 150 μm below a recess with a diameter of 300 μm and a length of 230 μm. Some free space for taking up the ejected droplet is provided adjacent to the orifice. The three dimensional structured grid consists of 148,956 cells. A 3D-grid was used despite the rotational symmetry of the problem to account properly for surface tension effects. Only the mirror symmetry has been exploited to reduce the model size. For driving the droplet generation a time dependent pressure boundary condition was applied at the top of the structure (*cf.* Fig. 8b). The pressure curve as depicted in Fig. 9 was determined by experiments with an integrated pressure sensor in the pneumatically actuated dispenser [72]. The walls at the nozzle outlet exhibit a contact angle of $\Theta = 130°$.

4.4.2. Droplet shape and tear off time

The natural qualitative measure to assess the simulation quality of droplet generation problems is the qualitative droplet shape during the droplet forming process. First of all the shape of a micro droplet can be determined very well by stroboscopic measurement techniques [4,5]. Second the correct prediction of the droplet shape requires consideration of all relevant physical effects (viscosity, surface tension etc.). Thus the transient droplet shape as displayed in Fig. 10 is ideally suited to test consistency with experiments. Furthermore the point in time at which the droplet detaches from the nozzle (tear-off time) is a valuable quantitative measure which can be extracted from stroboscopic experiments for validation purposes.

From the considered simulation tools Fluent and Flow-3D were not able to reproduce the droplet ejection in the TopSpot® case properly (*cf.* Fig. 10): The simulations performed with Fluent exhibit quite consistent results at the beginning of the ejection process, but fail to produce a free droplet like observed in the experiments. Even after increasing the driving pressure by 5% respectively 10% (*i.e.* scaling the values given in Fig. 9 by a factor of 1.05 respectively 1.10) no droplet release could be achieved. This result might be caused by an overestimation of the surface tension forces compared to body forces by the Fluent

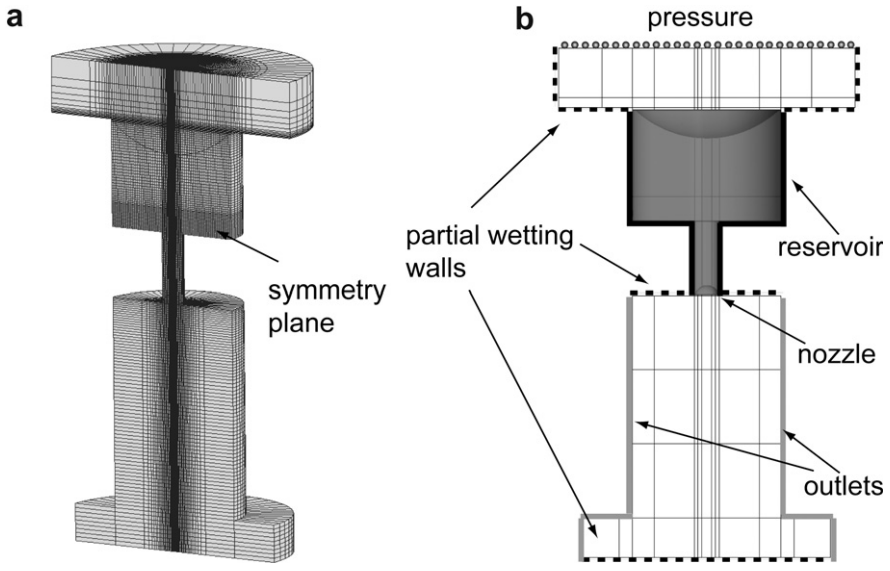

Fig. 8. Model of one TopSpot® nozzle. (a) Structured 3D mesh with symmetry plane in the middle. (b) Boundary conditions with a time dependent pressure boundary condition at the top (dotted line), partial wetting walls $\Theta = 130°$ (dashed and black lines) and outlets at the sides (grey lines), with the micro nozzle being filled with water (grey).

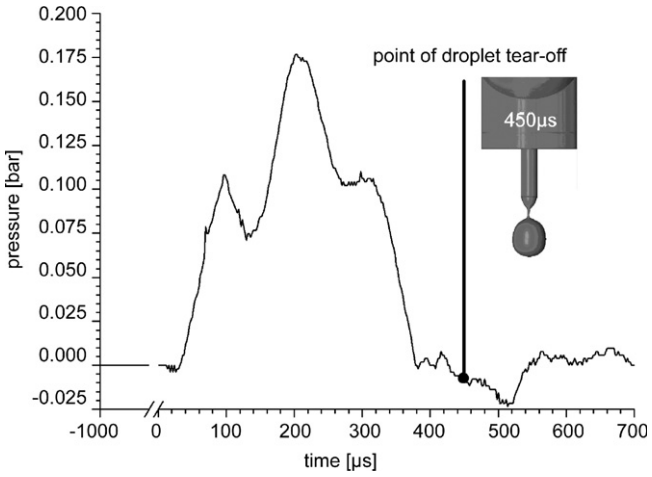

Fig. 9. Pressure pulse at the inlet from experiments.

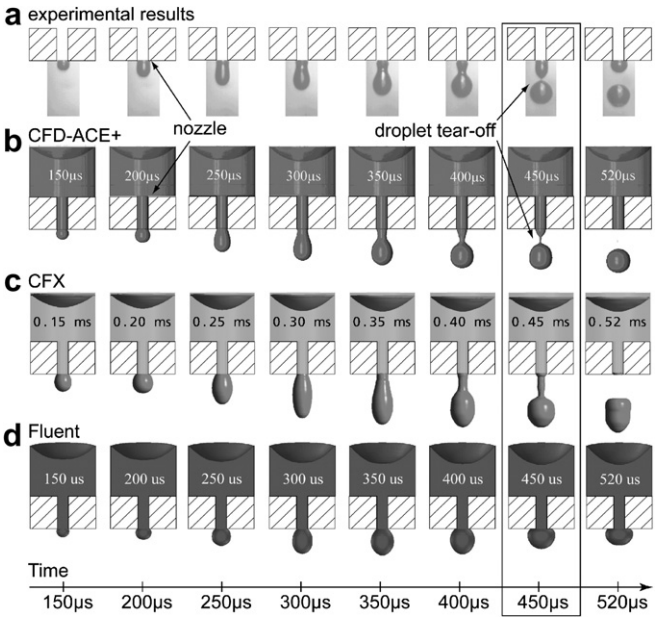

Fig. 10. Stroboscopic sequence of the droplet ejection process: (a) experimental results (showing only the orifice and the droplet); (b) CFD-ACE+ simulation results; (c) CFX simulation results; (d) Fluent simulation results. The point of tear-off is marked at 450 µs.

algorithm. This explanation would be in agreement with the consistent results obtained with Fluent for the equilibrium T-channel problem. As far as Flow-3D is concerned the authors could not achieve a successful implementation of the TopSpot® problem at all. Despite several intensive tries with similar effort like for the other tools no reasonable results could be obtained. Thus no assessment of Flow-3D can be presented for the TopSpot® case.

The remaining software tools CFD-ACE+ and CFX achieved both a successful droplet release with reasonable values for the tear-off time (450 µs for CFD-ACE+ and 500 µs for CFX). Best qualitative consistency with experiments in terms of droplet shape was achieved with CFD-ACE+ when applying a 5% higher pressure pulse than measured experimentally (*cf.* Fig. 10). The consistency of CFX with the experimental results is considerably weaker. Despite the fact, that also a 5% higher driving pulse was applied like for CFD-ACE+, the droplet tear-off is still delayed with respect to the experiment. Furthermore the correspondence of the simulation results to the experimental droplet shapes is much weaker. Like in the previous problem this observation can be explained by the less accurate surface reconstruction method adopted by CFX.

4.4.3. Droplet volume

The volume of the ejected droplet is one of the most important parameters regarding the design and operation of droplet generators. A stroboscopic camera was used to measure experimentally the dispensed volume of the flying droplet by evaluating the number of pixels of the droplet on the picture. For the precise analysis of the recorded pictures the image processing system NeuroCheck® [73] was used. The measurement error of the optically measured droplet volumes can be estimated to be ~5% due to the random error in the read out of the pixels representing one unit volume.

The ejected volume in the simulation is determined by the grid volume occupied by the droplet. For the successful determination of the droplet volume it has to be ensured that the droplet has teared off completely which was the case after 600 µs of simulation time (*cf.* Fig. 10). By this a volume of 0.66 nl was obtained for CFD-ACE+ which is in good agreement with the experimental result of 0.68 nl. The droplet volume calculated by CFX resulted in 1.4 nl which suggests that the applied surface reconstruction scheme tends to underestimate the surface tension forces compared to the body forces.

4.4.4. Comments on the simulations (TopSpot®)

For the proper assessment of the results it has to be pointed out that the TopSpot® dispenser has a very critical point of operation. That means only little changes in the viscosity or pressure can prevent a break up of the droplet. This high sensitivity constitutes a challenge for all simulation tools because small imbalances in rating the body forces versus the surface tension forces can result in large differences to the experimental values.

5. Computational speed

The assessment of computational speed provided in the following is only reflecting the performance of the studied software tools with respect to the closely defined benchmark problems presented in this work. It should be mentioned, that either software would most likely be able to simulate any of the problems faster. For most of the software tools the setup of the presented problems enforcing a structured grid and fixed times step are not the ideal settings to achieve maximum computational speed. Nevertheless, the values provided in Table 4 can serve to deduce the order of magnitude of the computational time required to

Table 4
Comparison of the computational times and maximum allocated memory of all problems and tools

	Split and recombine	Rotating channel	T-shaped channels	TopSpot®
CFD-ACE+				
CPU-Time [hh:mm:ss]	3:01:21	13:34:39	Design 1: 97:58:47 Design 2: 108:27:07 Design 3: 137:30:15	594:54:49
Max All. Memory [KB]	302.888	550.624	Design 1: 116.552 Design 2: 123.700 Design 3: 137.527	314.984
CFX				
CPU-Time [hh:mm:ss]	37:38:53	67:56:51	Design 1: 111:49:44 Design 2: 125:58:00 Design 3: 66:57:48	462:32:12
Max All. Memory [KB]	309.060	495.652	Design 1: 96.876 Design 2: 102.284 Design 3: 109.116	314.984
Flow-3D				
CPU-Time [hh:mm:ss]	83:12:00 (78:42:00 transient simulation, 04:30:00 constant velocity profile)	145:27:00 (133:28:00 transient simulation; 11:59:00 constant velocity profile)	Design 1: 11:04:00 Design 2: 14:41:00 Design 3: 13:48:00	NA
Max All. Memory [KB]	470.864	198.668	Design 1: 36.788 Design 2: 36.760 Design 3: 36.796	NA
Fluent				
CPU-Time [hh:mm:ss]	1:16:39	79:96:30[a]	Design 1: 31:22:43 Design 2: 49:30:05 Design 3: 51:49:57	634:24:48
Max All. Memory [KB]	239.368	530.408[a]	Design 1: 76.800 Design 2: 95.968 Design 3: 94.736	191.288

[a] After seven iterations as described in the text.

solve typical microfluidic problems involving mixing (stationary simulations) or free surfaces (transient simulations).

For the study of mixing problems and numerical diffusion the method of tracking the flow pattern with a scalar value has been chosen. Such problems typically require a steady-state solution. For Flow-3D only a transient solver was available for this purpose, therefore the tracking of the scalar value through the whole geometry results in long simulation times. A similar situation occurred in the simulations performed with Fluent for the rotating channel. In this case a manual iterative solution had to be applied, which increases the total computational time extremely compared to a standard stationary solution. Therefore these results are not directly comparable to the other tools.

For free surface problems simulated by the VOF method the computation time is of crucial importance. First of all the VOF algorithm (especially the surface reconstruction) adds considerably to the computational load. Second the capillary oscillation of the free surface which has to be resolved to obtain a convergent solution requires a very small time step (in the order of 10E−7 s to 10E−4 s) which is usually much too small for the typically required simulation times (in the order of 0.1 s to 10 s). Thus the simulation times are in total considerably longer than for stationary simulations and therefore the performance of computational speed is of particular interest.

To optimize the computational speed the size of the model should be as small as possible which first of all requires a good physical understanding of the problem under consideration. The only possibility inside the solver setup to increase the speed of the simulation process is to use automatic time stepping, non-iterative time steps or parallel processing if available. In some problems unstructured grids can also help to reduce computational time by minimising the number of computational cells. This can be especially beneficial for complex geometries but it becomes more difficult in combination with VOF, because the surface reconstruction algorithms are more complicated and costly on unstructured grids compared to structured grids. In the presented study all of these options to optimise the computational speed have not been exploited intentionally to keep the results as comparable as possible.

5.1. Computational time: split and recombine structure, rotating channel

In case of the split and recombine structure there are no special remarks on how to further speed-up the simulation process because all tools handle this case with reasonable simulation times. With ~1.25 h Fluent is the fastest tool

followed by CFD-ACE+ with ~3 h which is a factor of 2.4 slower. CFX and Flow-3D are the slowest tools in calculating the split and recombine structure where especially Flow-3D needs a factor of ~66 more time than the fastest tool Fluent. The reason for this is that Flow-3D does not provide a possibility to perform a steady-state simulation like explained before.

The rotating channel problem was somehow more challenging for the simulation tools because it needs a correct transformation of all boundary conditions and forces into the rotating system. CFD-ACE+ was easy to set-up but one has to be careful in using the correct boundary condition because only the inlets are transferred properly into the rotating system. With these settings CFD-ACE+ is the fastest tool in this case study and it is between five to ten times faster than the other tools. Fluent needs more time (factor 6) to simulate the rotating channel because an iterative method had to be used like described before to achieve a correct solution instead of one single solver run. For Flow-3D the need for a transient simulation in combination with the high aspect ratio of the rotating channel results in very long simulation times (comparable to the split and recombine structure).

5.2. Computation time: TopSpot®, T-shaped channel

Generally the VOF-method is very costly in terms of computational time. Nevertheless, the T-shape channel problem was calculated quite fast by Flow-3D. This might be due to the fact that the time stepping could not set to be constant for Flow-3D, while the other programs were restricted to fix time steps. Fluent is approximately a factor of 3 slower than Flow-3D, whereas the remaining programs needed between five to ten times more computation time.

For the extremely challenging TopSpot® problem CPU times between 463 h and 634 h have been determined. The simulation times differ by about a factor of 1.4, with CFX being the fastest tool. This is not amazing since no geometrical surface reconstruction is performed. Fluent is somewhat slower but as fast as CFD-ACE+. In general the calculation time for this type of problem could be improved by using a non-iterative time stepping method or adaptive time stepping. Especially the non-iterative time stepping method available in the current version of Fluent (6.2.16) is claimed to accelerate the simulation by a factor of more than five [74].

6. Conclusions

The presented results show that qualitatively all tools can perform well in calculating convection diffusion problems with a second order algorithm for the tracer scalar. The numerical diffusion is comparable and small for all tools and should allow for quantitative statements on flow patterning and lamination in mixing devices. Due to lack of experimental data a real quantitative assessment was not possible in this work.

In contrast to the case of mixing and flow patterning by convection and diffusion the microfluidic problems involving free surfaces and surface tension could not be simulated equally well with the considered programs. It turned out that CFX and Flow-3D did determine the free surface shapes not as correctly as the other programs. For CFX this can be attributed to the absence of geometrical surface reconstruction methods, for Flow-3D the reason for that remains unclear. While for the problem of the bubble in the T-shaped channel the deviations from experiments were generally small, they became considerable for the TopSpot droplet generation problem. The droplet break off could only be reproduced correctly by CFD-ACE+. In contrast to the other tools CFD-ACE+ does offer an adjustable surface damping. This in combination with the high order surface reconstruction scheme might be the reason for the good performance in that case. Generally CFD-ACE+ as well as Fluent can be recommended for simulation of free surface flows involving capillary forces. Nevertheless, it has to be acknowledged that for complex problems a careful modelling and validation of the simulations has to be carried out before quantitative results can be expected like shown in this case study.

The considerations with respect to the computational speed as provided here do not justify a general conclusion. To enable a thorough assessment of the computational speed each of the programs has to be operated at its optimum capabilities, making use of features like automatic time stepping, parallel processing, adaptive automatic grid generation etc. This would have been far beyond the scope of this work. Therefore no comparative conclusions should be drawn from the assessment of the computational speed. Nevertheless it can be stated that the simulation times obtained by all tools – ranging from a few hours for stationary problems and up to 600 hours for the very complex transient TopSpot problem – justify their use as engineering tool for the considered type of microfluidic problems.

Acknowledgements

The authors want to thank all of the mentioned companies for supplying their software products for this case study, partly free of costs. Without their help and excellent support it would have been very difficult for the authors to introduce themselves quickly to the various software packages and to set up the simulation problems. Part of this work was supported by the German Federal Ministry of Education and Research (BMBF) within the Micro-DMFC-Project (no. 03SF0311B) which is gratefully acknowledged.

Appendix A

See Tables A.1 and A.2.

Table A.1
Solver settings flow patterning

Boundary conditions	Split and recombine	Rotating channel
Density ρ of fluid 1 (water)	977 kg m^{-3}	977 kg m^{-3}
Viscosity μ of fluid 1 (constant, dynamic)	8.55E−4 kg m^{-1} s^{-1}	8.55E−4 kg m^{-1} s^{-1}
Solver and solver related settings		
Time dependency	Steady state	Steady state
Number of time steps	–	–
Time step size	–	–
Time accuracy	Euler (first order)	Euler (first order)
Maximum number of iterations	1000	1500
Convergence criteria	1E−4	1E−5
Minimum residual	1E−18	1E−18
Spatial differencing (flow module)	Second order, limiter 0.1	Second order, limiter 0.1
Spatial differencing (scalar module)	Second order, blending 0.1	Second order, blending 0.1
Scalar settings		
Diffusivity scalar	2E−20 s m^{-2}	2E−20 s m^{-2}
Specific settings:		
Angular velocity (w_z)		100 rad s^{-1}
Pressure		0 Pa
Velocity		0 m s^{-1}
Symmetry		XY-plane
Wall		
Inlets	Fixed flow boundary conditions	

Table A.2
Solver settings free surfaces (VOF)

Boundary conditions	T-shaped channel	Top-spot
Density ρ_1 of fluid 1 (air)	1.1614 kg m^{-3}	1.1614 kg/m^3
Viscosity μ of fluid 1 (constant, dynamic)	1.846E−5 kg m^{-1} s^{-1}	1.846E−5 kg m^{-1} s^{-1}
Density ρ_2 of fluid 2 (water)	1000 kg m^{-3}	1000 kg m^{-3}
Viscosity ν of fluid 2 (constant, kinematic)	1E−6 m^2 s^{-1}	1E−6 m^2 s^{-1}
Surface tension σ	0.0725 N m^{-1}	0.0725 N m^{-1}
Solver and solver related settings		
Time dependency	Transient (equilibrium)	Transient (dynamic)
Number of time steps	4000	12,000
Time step size	2E−6	4E−007
Convergence criteria	1E−4	1E−4
Spatial differencing	Upwind, first order	Upwind, first order
VOF		
Surface reconstruction method	Second order (PLIC)	Second order (PLIC)
Pressure	Second order	Second order
Specific settings		
Contact angle Θ – wall	5° (channels end and side walls)	130°
Symmetry		

References

[1] Anderson JD. Computational fluid dynamics. 1st ed. McGraw-Hill Science/Engineering/Math; 1995.

[2] Versteeg HK, Malalasekera M. An introduction to computational fluid dynamics, the finite volume method. Prentice-Hall; 1996.

[3] Erickson D. Towards numerical prototyping of labs-on-chip: modeling for integrated microfluidic devices. Microfluid Nanofluid 2005;1(4):301–18.

[4] Frohn A, Roth N. Dynamics of droplets. 1st ed. Berlin/Heidelberg: Springer-Verlag; 2000. p. 1–292.

[5] Lee ER. Microdrop generation. 1st ed. Boca Raton: CRC Press; 2002. p. 1–251.

[6] Tarnogrodzki A. Theoretical prediction of the critical weber number. Int J Multiphase Flow 1993;19(2):329–36.

[7] Hirt CW, Nichols BD. Volume of fluid (Vof) method for the dynamics of free boundaries. J Comput Phys 1981;39(1):201–25.

[8] Annaland MV, Deen NG, Kuipers JAM. Numerical simulation of gas bubbles behaviour using a three-dimensional volume of fluid method. Chem Eng Sci 2005;60(11):2999–3011.

[9] Kothe DB, Rider WJ. Comments on modeling interfacial flows with volume-of-fluid methods. Los Alamos National Laboratory, Technical Report LA-UR-94-3384; 1995.

[10] Lorstad D, Fuchs L. High-order surface tension VOF-model for 3D bubble flows with high density ratio. J Comput Phys 2004;200(1):153–76.

[11] Brackbill JU, Kothe DB, Zemach C. A continuum method for modeling surface-tension. J Comput Phys 1992;100(2):335–54.
[12] Nguyen NT, Wu ZG. Micromixers – a review. J Micromech Microeng 2005;15(2):R1–R16.
[13] Hardt S, Schonfeld F. Laminar mixing in different interdigital micromixers: II. Numerical simulations. AIChE J 2003;49(3):578–84.
[14] Hessel V, Hardt S, Lowe H, Schonfeld F. Laminar mixing in different interdigital micromixers: I. Experimental characterization. AIChE J 2003;49(3):566–77.
[15] Johnson TJ, Ross D, Locascio LE. Rapid microfluidic mixing. Anal Chem 2002;74(1):45–51.
[16] Cupelli C, Koltay P, Santer M, Zengerle R. Compact model of a laminar micro mixer. In: Technical proceedings of the 2005 nanotechnology conference and trade show; 2005. p. 724–27.
[17] Cupelli C, Koltay P, Ducree J, Zengerle R, Santer M. Towards a modular split & recombine micro mixer. In: Proceedings of the eighth international conference on microreaction technology (IMRET); 2005.
[18] Ottino JM, Wiggins S. Introduction: mixing in microfluidics. Philo Trans Roy Soc London Ser A – Math Phys Eng Sci 2004;362(1818): 923–35.
[19] Hardt S. An extended volume-of-fluid method for micro flows with short-range interactions between fluid interfaces. Phys Fluids 2005;17(10).
[20] Sussman M, Smereka P, Osher S. A level set approach for computing solutions to incompressible 2-phase flow. J Comput Phys 1994;114(1): 146–59.
[21] "Coventor, Inc."; 2006.
[22] "COMSOL, Inc."; 2006.
[23] Freitas CJ. Perspective – selected benchmarks from commercial Cfd codes. J Fluids Eng – Trans ASME 1995;117(2):208–18.
[24] Horvat A, Kljenak I, Marn J. On incompressible buoyancy flow benchmarking. Numer Heat Transfer Part B – Fundam 2001;39(1): 61–78.
[25] Iaccarino G. Prediction of the turbulent flow in a diffuser with commercial CFD codes. Center for Turbulence Research Annual Research Briefs 2000:271–8.
[26] Lindemann T, Sassano D, Bellone A, Zengerle R, Koltay P, Three-dimensional CFD-simulation of a thermal bubble jet printhead. In: NSTI nanotechnology conference and trade show, 2nd ed.; 2004. p. 227–30.
[27] Lindemann T, Streule W, Birkle G, Zengerle R, Koltay P. PipeJet^{Tm} – a simple disposable dispenser for the nanoliter range. In: Actuator 2004, 1st ed.; 2004, p. 224–27.
[28] Lindemann T, Ashauer H, Goettsche T, Sandmaier H, Yu Y, Peters R-P, Sassano D, Bellone A, Scardovi A, Zengerle R, Koltay P. Thermal bubble jet printhead with integrated nozzle plate. In: NIP20, international conference on digital printing technologies. 1st ed.; 2004, p. 834–39.
[29] Ferziger JH, Peric M. Computational methods for fluid dynamics. 3rd ed. Springer; 2002.
[30] CFD-ACE+ (ESI-Group). CFD-ACE+ (ESI-Group); 2004.
[31] CFX; 2004.
[32] Flow-3D (Flow Science, Inc); 2004.
[33] Fluent Inc., Fluent (Fluent Inc.); 2005.
[34] Flow-3D (Flow Science, Inc), User's Manual; 2004.
[35] Vandoormaal JP, Raithby GD. Enhancements of the simple method for predicting incompressible fluid-flows. Numer Heat Transfer 1984;7(2):147–63.
[36] Barkhudarov MR, Chin SB. Stability of a numerical algorithm for gas bubble modeling. Int J Numer Methods Fluids 1994;19(5): 415–37.
[37] Barkhudarov MR. Semi-Lagrangian VOF advection method for FLOW-3D. Flow Science Technical Note, vol. (FSI-03-TN63); 2003.
[38] Hirt CW, Nichols BD, Romero NC. "SOLA – a numerical solution algorithm for transient fluid flows. Los Alamos National Laboratory Report, vol. LA-5852; 1975.
[39] Nichols BD, Hirt CW, Hotchkiss RS. SOLA-VOF: a solution algorithm for transient fluid flow with multiple free boundaries. Los Alamos National Laboratory Report, vol. LA-8355; 1980.
[40] Pilliod JE, Puckett EG. Second-order accurate volume-of-fluid algorithms for tracking material interfaces. J Comput Phys 2004;199(2):465–502.
[41] Rider WJ, Kothe DB, Mosso SJ, Cerutti JH, Hochstein JI. Accurate solution algorithms for incompressible multiphase flows. Presented at the 33rd AIAA aerospace science meeting and exhibit, AIAA-95-0699; October 1994.
[42] Zwart PJ, Scheurer M, Bogner M, FREE surface flow modelling of an impinging jet. In: ASTAR international workshop on advanced numerical methods for multidimensional simulation of two-phase flow. GRS Garching, Germany; 2003.
[43] Anghaie S, Chen G. Adoption of single-phase CFD to two-phase flow and heat transfer problems 2000.
[44] Cummins SJ, Francois MM, Kothe DB. Estimating curvature from volume fractions. Comput Struct 2005;83(6-7):425–34.
[45] Eggers J. Theory of drop formation. Phys Fluids 1995;7(5):941–53.
[46] Trottenberg U, Oosterlee CW, Schüller A. Multigrid. Academic Press; 2001.
[47] Sonneveld P. Cgs, a fast Lanczos-type solver for nonsymmetric linear-systems. SIAM J Sci Stat Comput 1989;10(1):36–52.
[48] Python 2.3.3; 2005.
[49] Kothe DB, Rider WJ, Mosso SJ, Brock JS, Hochstein J.I. Volume tracking of interfaces having surface tension in two and three dimensions. In: Presented at the 34rd aerospace sciences meeting and exhibit, Technical Report AIAA 96-0859, January1996.
[50] AI*Environment; 2005.
[51] ICEM CFD; 2005.
[52] "MPI – Message-Parcing Interface"; 2006.
[53] Geist G, Kohl J, Papadopoulos P. PVM and MPI: a comparison of features. Calcul Paralleles 1996;8(2):137–50.
[54] Fluent Inc., Gambit 2.1 Documentation; 2003.
[55] Fluent Inc., Fluent 6.1 Documentation; 2003.
[56] SysInternals PsList; 2006.
[57] ESI CFD, Inc., Huntsville, AL, Material Database, CFD-ACE+; 2004.
[58] Madou M, Lee L, Daunert S, Lai S, Shih C. Design and fabrication of CD-like microfluidic platforms for diagnostics. Biomed Microdev 2001;3(3):245–54.
[59] Brenner T, Glatzel T, Zengerle R, Ducrée J. Frequency-dependent transversal flow control in centrifugal microfluidics. Lab on a chip 2005;5(2):146–50.
[60] Ducree J, Haeberle S, Brenner T, Glatzel T, Zengerle R. Patterning of flow and mixing in rotating radial microchannels. Microfluid Nanofluid 2005;2(2):97–105.
[61] Haeberle S, Brenner T, Schlosser HP, Zengerle R, Ducrée J. Centrifugal micromixer. Chem Eng Technol 2005;28(5):613–6.
[62] Ducrée J, Brenner T, Haeberle S, Glatzel T, Zengerle R. Multilamination of flows in planar networks of rotating microchannels. Microfluid Nanofluid 2006;2(1):78–84.
[63] Kim DS, Kwon TH. Modeling, analysis and design of centrifugal force-driven transient filling flow into a circular microchannel. Microfluid Nanofluid 2006;2(2):125–40.
[64] Kohnle J, Waibel G, Cernosa R, Storz M, Ernst H, Sandmaier H, Strobelt T, Zengerle R. A unique solution for preventing clogging of flow channels by gas bubbles. In: IEEE MEMS, The 15th international IEEE micro electro mechanical conference ed. Las Vegas; 2002. p. 77–80.
[65] Litterst C, Kohnle J, Ernst H, Messner S, Sandmaier H, Zengerle R, Koltay P. Mobility of gas bubbles in CHIC-type flow channels. In: H. Borgmann, editor, ACTUATOR; 2004, p. 541–44.
[66] Waibel G, Kohnle J, Cernosa R, Storz M, Schmitt M, Ernst H, et al. Highly integrated autonomous microdosage system. Sens Actuators A – Phys 2003;103(1-2):225–30.
[67] Litterst C, Eccarius S, Hebling C, Zengerle R, Koltay P. Increasing μDMFC efficiency by passive CO_2 bubble removal and discontinuous operation. J Micromech Microeng 2006;16(9):S248–253, Aug. 2006.